ELSEVIER

Contents lists available at ScienceDirect

Soil Dynamics and Earthquake Engineering

journal homepage: www.elsevier.com/locate/soildyn





Measurement of dynamic properties of rubber-sand mixtures across wide strain amplitudes by combined resonant column and cyclic simple shear tests

Wei Liang^a, Mengtao Wu^b, Fangcheng Liu^{a,*}, Kai Zheng^a, Jun Yang^c, Jie He^a

- ^a College of Civil Engineering, Hunan University of Technology, Zhuzhou, China
- ^b Department of Civil Engineering, Sichuan University, Chengdu, China
- ^c Department of Civil Engineering, The University of Hong Kong, Pokfulam, Hong Kong

ARTICLE INFO

Keywords: Rubber-sand mixtures Dynamic properties Wide strain amplitudes Particle size ratio Resonant column test Cyclic simple shear test

ABSTRACT

The systematic exploration of the dynamic characteristics of various rubber-sand mixtures (RSM) across a wide range of strain amplitudes $(10^{-6} \sim 10^{-1})$ addresses a pivotal challenge in the deployment of recycled waste tires as an economical, energy-absorbing material in geotechnical earthquake engineering. This study aims to elucidate the dynamic characteristics of this distinctive soil under wide strains and explores the appropriate particle size selection, optimal ratio, and initial state parameters for RSM as a geotechnical seismic isolation system. The investigation initiates with a series of resonant column tests to determine the dynamic shear modulus and damping ratio of RSM at small strain amplitudes, considering different rubber contents (RC), particle size ratios (PSR), and confining pressures. Subsequently, cyclic simple shear tests with larger strain amplitudes were conducted to examine the dynamic properties of RSM across a wide range of shear strains. The results indicate that: The PSR of rubber to sand significantly influences the dynamic parameters of RSM at small strains, resulting in a 3-4 fold change in the maximum dynamic shear modulus, which is attenuated at large strains, and exhibiting a coupling effect between the PSR and RC on the dynamic shear modulus and damping ratio. Over a wide strain amplitude range, including rubber particles enhances the damping characteristics of sandy soil. At small strains, the damping ratio gradually increases with the rise in RC; however, under large strain conditions, the variation trend of the damping ratio depends on the specific RC. when the RC increases from 0 % to 25 %, the dynamic shear modulus of RSM decreases significantly. As the RC further increases to 30 %, the extent of reduction in the dynamic shear modulus decreases significantly. These findings on the dynamic behavior of RSM under different strain conditions are crucial for guiding future theoretical research and engineering applications in seismic protection.

1. Introduction

The rapid growth of the global industry, especially the automobile sector, has led to an increasing accumulation of end-of-life tires. This highlights the need for improved recycling and treatment methods to efficiently manage this hard-to-degrade solid waste. Incomplete recycling of waste tires poses significant environmental challenges, such as occupying large land areas [1,2]. To address this issue, researchers have explored the potential of utilizing waste tires in engineering applications due to their unique mechanical properties, such as high elasticity and energy absorption [3–6].

One possible option is to convert scrap tires into rubber granules that can be mixed with sand particles to form rubber-sand mixtures (RSM). RSM exhibits several beneficial qualities. Research has shown that RSM has a lower density, higher elastic deformation capacity, and increased energy absorption. These properties make RSM suitable for various civil engineering applications [7,8], including soft foundation treatment, retaining walls, and backfill for pipelines and culverts. Furthermore, RSM can be used as a low-cost energy absorber, making it ideal for seismic isolation applications, a use supported by numerical calculations [9–14] and experimental studies [15–19] performed by many researchers.

E-mail addresses: weilianghut@163.com (W. Liang), mtwu@scu.edu.cn (M. Wu), fcliu@hut.edu.cn (F. Liu), kaizhenghut@163.com (K. Zheng), junyang@hku.hk (J. Yang), hejie76@hut.edu.cn (J. He).

https://doi.org/10.1016/j.soildyn.2025.109536

^{*} Corresponding author.

Table 1
Summary of previous and current studies on the dynamic behavior of RSM.

Research worker	Particular year	Dynamic parameters studied	Shear strain amplitudes	Laboratory instruments
Feng and Sutter [20].	2000	Shear modulus, Damping	$10^{-6} \sim 5 \times 10^{-4}$	Resonant column
Lee et al. [21]	2007	ratio Maximum dynamic shear modulus	10 ⁻⁶	Bendesr elements
Lee et al. [22]	2010	$(G_{ m dmax})$ $G_{ m dmax}$	10^{-6}	Bender
Senetakis et al. [23]	2012	Shear modulus, Damping ratio	$10^{-5} \sim 5 \times 10^{-4}$	elements Resonant column
Anastasiadis et al. [24]	2012	$G_{ m dmax}$, Initial damping ratio	$\begin{array}{l} 5 \times 10^{-6} {\sim} 5 \\ \times 10^{-4} \end{array}$	Resonant column
Nakhaei et al. [25]	2012	$G_{ m dmax}$, Shear modulus, Damping	$10^{-4} \sim 10^{-2}$	Cyclic triaxial
Bahadori and Manafi [26]	2013	Shear modulus, Damping ratio	$10^{-3} \sim 10^{-1}$	Shaking table
Ehsani et al. [27]	2015	Shear modulus, Damping ratio	$\begin{array}{l} 4 \times \\ 10^{-6} \text{\sim} 2.7 \\ \times \ 10^{-2} \end{array}$	Resonant column and cyclic triaxial
Li et al. [28]	2016	Shear modulus, Damping ratio	$10^{-6} \sim 10^{-1}$	Resonant column and cyclic triaxial
Mashiri et al. [29]	2016	$G_{ m dmax}$	$10^{-3}{\sim}10^{-2}$	Cyclic triaxial
Madhusudhan et al. [30]	2017	Shear modulus, Damping ratio	$0.2 \times 10^{-2} \sim 3 \times 10^{-2}$	Cyclic triaxial
Okur and Umu [31].	2018	$G_{ m dmax}$, Shear modulus, Damping ratio	$8 \times 10^{-6} \sim 10^{-3}$	Resonant column and dynamic torsional shear system
Pistolas et al. [32]	2018	Shear modulus, Damping ratio	$10^{-5} \sim 10^{-2}$	Resonant column and cyclic triaxial
Sarajpoor et al. [33]	2020	Shear modulus, Damping ratio	10 ⁻⁴ ~10 ⁻²	Cyclic hollow cylinder
Das and Bhowmik [34]	2020	$G_{ m dmax}$, Shear modulus, Damping ratio	$10^{-5} \sim 10^{-4}$	Torsional resonant column
Das and Bhowmik [35].	2020	$G_{ m dmax}$, Shear modulus, Damping ratio	$10^{-5} \sim 6 \times 10^{-4}$	Resonant column
Li et al. [36]	2020	$G_{ m dmax}$, Shear modulus, Damping ratio	$10^{-4} \sim 5 \times 10^{-2}$	Cyclic triaxial
Rios et al. [37]	2021	$G_{ m dmax}$, Shear modulus, Damping ratio	$10^{-5} \sim 5 \times 10^{-2}$	Bender elements and cyclic triaxial
Wu et al. [38]	2021	Shear modulus, Damping ratio	$10^{-6} \sim 5 \times 10^{-3}$	Resonant column

Table 1 (continued)

Research worker	Particular year	Dynamic parameters studied	Shear strain amplitudes	Laboratory instruments
Ghazavi and Kavandi [39].	2022	Shear modulus, Damping ratio	$10^{-2} \sim 10^{0}$	Cyclic triaxial
Banzibaganye and Vrettos [40].	2022	$G_{ m dmax}$, Shear modulus, Damping ratio	$10^{-6} \sim 5 \times 10^{-3}$	Resonant column
Wu et al. [41]	2023	$G_{ m dmax}$, Shear modulus, Damping ratio	$10^{-2} \sim 6 \times 10^{-2}$	Cyclic simple shear
Kowalska and Vrettos [42].	2025	$G_{ m dmax}$, Shear modulus, Damping ratio	$10^{-6} \sim 10^{-4}$	Resonant column
Present study	2025	$G_{ m dmax}$, Shear modulus, Damping ratio	$10^{-6} \sim 10^{-1}$	Resonant column and cyclic simple shear

Numerous scholars have conducted comprehensive studies on RSM, particularly focusing on the dynamic properties through a significant number of experimental investigations. Table 1 presents a systematic categorization of past research on the dynamic properties of RSM based on the year, dynamic parameters, range of shear strains (γ_d), and experimental equipment used. It also lists the specifications of the tests in the current study for comparative analysis. Existing experimental studies on the dynamic properties of RSM generally show that the dynamic shear modulus of RSM decreases while the damping ratio increases with higher rubber content (RC is the percentage of rubber mass to RSM mass, $RC = m_{\text{rubber}}/m_{\text{RSM}} \times 100$ %). However, there is no consensus on the impact of particle size ratio ($PSR = D_{50,\text{rubber}}/D_{50,\text{sand}}$) on the dynamic properties of RSM. As a result, a comprehensive understanding of the factors influencing the dynamic properties is still lacking. Furthermore, although extensive studies have been conducted on the dynamic characteristics of RSM under small and large strain amplitudes, there is a limited understanding of the effects of PSR, RC, and confining pressure on the nonlinear dynamic characteristics of RSM under wide strain amplitudes.

It collected and analyzed extensive test data through resonant column tests and cyclic simple shear tests. This study comprehensively revealed the nonlinear dynamic characteristics of RSM under wide strain amplitudes, analyzed the coupling effects of different influencing factors, and further examined the deformation mechanisms of RSM. The remainder of this paper is organized as follows: Section 2 provides detailed information about the control parameters of the sample, preparation process, and test procedure; Section 3 presents an in-depth analysis of the effects of *PSR*, confining pressure, and *RC* on the dynamic shear modulus and damping ratio of RSM under wide strain amplitudes; Section 4 summarizes some major conclusions.

2. Sample preparation and test procedure

2.1. Materials

The rubber particles used in this study were derived from recycled waste tires, consistent with most existing research. Therefore, the findings of our study are widely applicable to rubber particles produced from crushed waste tires. However, for rubber particles of other origins, further analysis and comparison are required. The specific gravity of rubber particles is 1.1. The sand used in the tests was Fujian sand (Chinese ISO standard sand). The specific gravity of sand is 2.67, and Fig. 1 shows the rubber particles and sand particles used in this study.

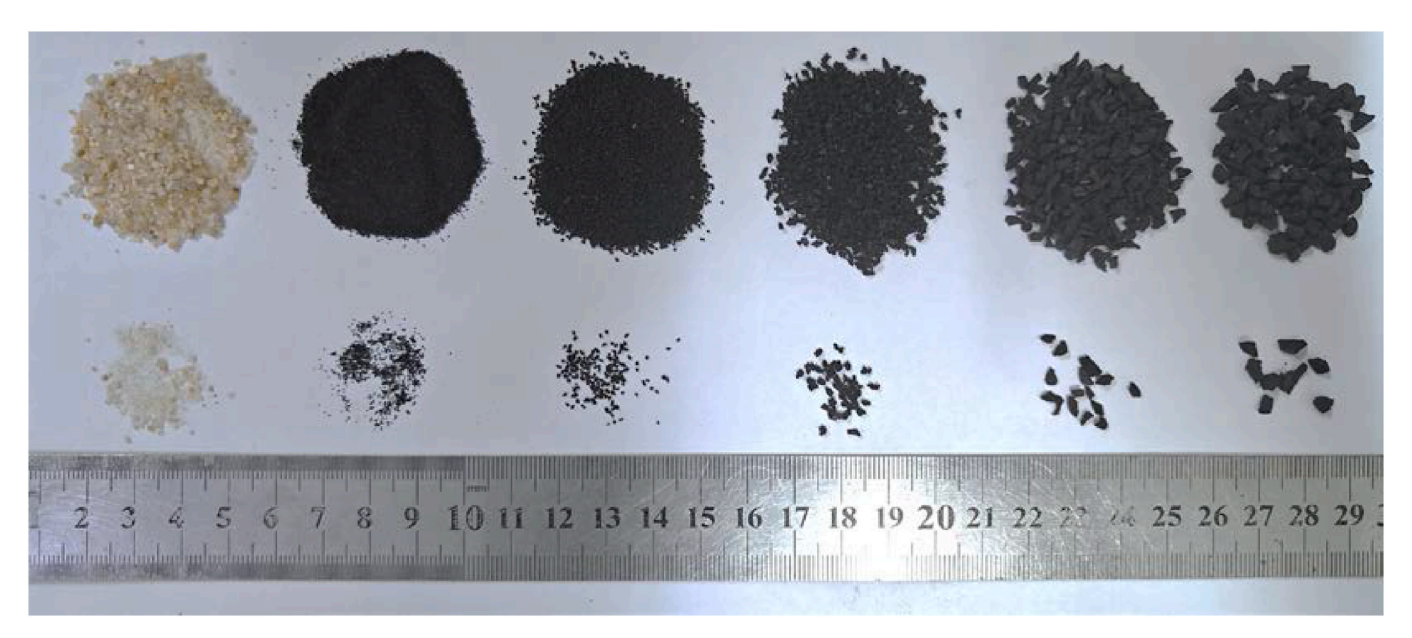


Fig. 1. Close-up view of standard sand and varied rubber particle sizes.

Table 2Median particle diameter and coefficient of uniformity of sand and rubber particles.

Physical properties	Materia	ıls												
	FJS	R0.2	R0.3	R0.6	R0.64	R1.18	R1.6	R1.9	R2.0	R2.36	R3	R3.45	R3.7	R4.75
D ₅₀	0.64	0.2	0.3	0.6	0.64	1.18	1.6	1.9	2.0	2.36	3.0	3.45	3.7	4.75
$C_{ m u}$	4.33	2.44	2.10	1.98	2.07	2.89	1.37	1.61	2.19	3.06	1.27	1.22	1.14	1.27
C_{c}	0.72	1.02	0.86	0.87	0.89	1.00	0.94	0.92	0.97	1.03	0.95	0.98	0.98	1.01

The basic physical properties of the sand and rubber particles were measured according to the GB/T 50123-2019 [43] standard in the geotechnical laboratory of Hunan University of Technology. The physical properties of the materials are listed in Table 2, Tables 3, and Table 4. In Tables 3 and 4, the testing materials are labeled as follows: "R" represents rubber particles, with the number following it indicating the median particle diameter (D_{50}) of the rubber. "FJS" stands for Fujian sand, with the subsequent number denoting the median particle diameter of the sand. The final standalone number indicates the mass percentage of rubber in the mixture. For example, the sample "R0.2-FJS0.64-5" signifies rubber particles with a median size of 0.2 mm, Fujian sand with a median size of 0.64 mm, and an RC of 5 %.

Previous studies [44,45] have demonstrated that the coefficient of uniformity significantly affects the dynamic properties of sand particles. As shown in Table 2, the coefficient of uniformity of the standard sand used in this study is 4.33, indicating a wide grain size distribution that includes various particle sizes. In comparison, the coefficient of uniformity for rubber particles ranges from 1.14 to 3.06, reflecting a relatively uniform grain size distribution with smaller variations in particle size. From the grain size distribution curve shown in Fig. 2, it can be observed that the sand particles used in this study predominantly fall within the size range of 0.1–1.0 mm, Overall, rubber particles exhibit a more uniform grain size distribution than standard sand.

2.2. Testing equipment

The instrument used to assess the dynamic characteristics of RSM at small shear strain ($\gamma_d=10^{-6}{\sim}10^{-4}$) amplitudes is the GDS resonant column test device (Fig. 3a). The theory and practical application of the resonant column test are extensively documented in numerous sources [46]. The dynamic characteristics of each sample can be assessed through controlled tests conducted at varying confining pressures. The

isotropic confining pressure was gradually increased from $50\,\mathrm{kPa}$ to $200\,\mathrm{kPa}$ and the shear modulus and damping characteristics were measured at each stage. The sample dimensions are: $50\,\mathrm{mm}$ in diameter and $100\,\mathrm{mm}$ in height.

The dynamic properties of RSM were measured under large shear strain conditions $(\gamma_d=5\times 10^{-4}{\sim}5\times 10^{-2})$ using the WF25735 cyclic simple shear test system from the British WFI company (Fig. 3b). This system includes a simple shear instrument, transducer, and computer system. The specimens, with a diameter of 70 mm and a height of 20 mm, are wrapped in a rubber membrane and surrounded by thin copper rings to simulate boundary conditions. This setup allows for shear testing under fixed volume, fixed vertical pressure, strain-controlled, and stress-controlled conditions. The displacement sensor has an accuracy of 1 μ m, and the force sensor can measure accurately up to 0.001 kN. The test system allows for setting the number of shear cycles for each level of strain amplitude, collecting 50 measurement points per cycle.

2.3. Sample preparation

Resonant column test: The sample preparation process was conducted under dry conditions. Six different percentages were utilized: 5%, 10%, 15%, 20%, 25%, and 30%, with pure sand as a control. The mixture is evenly divided into five parts by mass after thoroughly mixing rubber and sand to ensure uniformity. The mixture is gradually loaded into the mold in five increments using a long-neck funnel. After each loading, the sample is struck with a hammer until reaching the desired height (20~mm), and grooves are scraped onto the surface of previous layers to reduce stratification.

Cyclic simple shear test: The sample preparation process is conducted under dry conditions. The dried Fujian sand and air-dried rubber granules/powder were mixed according to specified mass ratios. The resulting mixture was then placed into sealed soil containers for future

Table 3Test conditions and basic physical properties of samples for the resonant column test.

Test materials	$PSR (D_{r,50}/D_{s,50})$	RC (%)	Max. dry density (g/cm³)	Min. dry density (g/cm ³)	Controlled dry density (g/cm³)	Relative density	Specimen mass (g)
FJS0.64-0	_	0	1.96	1.70	1.88	0.7	368.4
R0.2-FJS0.64-5	0.3 = 0.2/0.64	5	1.78	1.47	1.68	0.7	329.1
R0.2-FJS0.64-10		10	1.71	1.30	1.56	0.7	320.0
R0.2-FJS0.64-20		20	1.41	1.07	1.29	0.7	253.7
R0.2-FJS0.64-25		25	1.23	0.90	1.09	0.7	213.6
R0.3-FJS0.64-5	0.5 = 0.3/0.64	5	1.79	1.46	1.65	0.7	323.9
R0.3-FJS0.64-10		10	1.70	1.29	1.55	0.7	304.5
R0.3-FJS0.64-15		15	1.53	1.18	1.41	0.7	276.0
R0.3-FJS0.64-30		30	1.13	0.82	1.01	0.7	198.6
R0.6-FJS0.64-5	0.9 = 0.6/0.64	5	1.75	1.49	1.66	0.7	326.2
R0.6-FJS0.64-10		10	1.55	1.32	1.47	0.7	288.9
R0.6-FJS0.64-15		15	1.43	1.16	1.33	0.7	262.0
R0.6-FJS0.64-30		30	1.07	0.82	0.98	0.7	193.2
R0.64-FJS0.64-5	1.0 = 0.64/0.64	5	1.75	1.49	1.66	0.7	326.6
R0.64-FJS0.64-		10	1.55	1.32	1.47	0.7	287.8
10							
R0.64-FJS0.64-		20	1.30	1.02	1.20	0.7	236.9
15							
R0.64-FJS0.64-		25	1.20	0.92	1.10	0.7	217.9
25							
R1.6-FJS0.64-5	2.5 = 1.6/0.64	5	1.83	1.59	1.75	0.7	343.7
R1.6-FJS0.64-10		10	1.73	1.50	1.66	0.7	320.6
R1.6-FJS0.64-15		20	1.50	1.32	1.44	0.7	282.9
R1.6-FJS0.64-25		25	1.40	1.19	1.34	0.7	263.4
R1.9-FJS0.64-5	3.0 = 1.9/0.64	5	1.83	1.59	1.75	0.7	343.5
R1.9-FJS0.64-10		10	1.74	1.50	1.66	0.7	326.6
R1.9-FJS0.64-15		15	1.65	1.41	1.57	0.7	308.2
R1.9-FJS0.64-30		30	1.31	1.14	1.25	0.7	246.4
R3.0-FJS0.64-5	4.7 = 3.0/0.64	5	1.83	1.61	1.76	0.7	345.1
R3.0-FJS0.64-10		10	1.77	1.55	1.70	0.7	320.1
R3.0-FJS0.64-15		20	1.60	1.35	1.51	0.7	297.7
R3.0-FJS0.64-25		25	1.52	1.27	1.43	0.7	281.9
R3.7-FJS0.64-5	5.8 = 3.7/0.64	5	1.83	1.61	1.76	0.7	345.8
R3.7-FJS0.64-10		10	1.77	1.55	1.70	0.7	334.1
R3.7-FJS0.64-15		15	1.69	1.43	1.61	0.7	315.4
R3.7-FJS0.64-30		30	1.61	1.32	1.51	0.7	266.9

Table 4Test conditions and basic physical properties of samples for the cyclic simple shear test.

Test materials	$PSR (D_{\rm r,50}/D_{\rm s,50})$	RC (%)	Max. dry density (g/cm³)	Min. dry density (g/cm ³)	Controlled dry density (g/cm³)	Relative density	Specimen mass (g)
FJS0.64-0	_	0	1.96	1.70	1.88	0.65	144.7
R2.6-FJS0.64-10	3.1 = 2.0/0.64	10	1.75	1.21	1.51	0.65	116.2
R2.6-FJS0.64-20		20	1.51	1.04	1.30	0.65	100.0
R2.6-FJS0.64-30		30	1.42	0.92	1.19	0.65	91.5
R0.2-FJS0.64-5	0.3 = 0.2/0.64	5	1.78	1.47	1.68	0.65	129.3
R0.2-FJS0.64-10		10	1.71	1.30	1.56	0.65	120.1
R0.2-FJS0.64-15		15	1.50	1.14	1.35	0.65	103.9
R0.2-FJS0.64-20		20	1.41	1.07	1.29	0.65	99.3
R0.2-FJS0.64-25		25	1.23	0.90	1.09	0.65	83.9
R0.2-FJS0.64-30		30	1.02	0.71	0.88	0.65	67.7
R0.6-FJS0.64-30	0.9 = 0.6/0.64	30	1.07	0.82	0.98	0.65	75.4
R1.18-FJS0.64- 30	1.8 = 1.18/0.64	30	1.19	0.92	1.08	0.65	83.1
R2.36-FJS0.64- 30	3.7 = 2.36/0.64	30	1.25	0.97	1.14	0.65	87.7
R3.45-FJS0.64- 30	5.2 = 3.45/0.64	30	1.30	1.01	1.18	0.65	90.8
R4.75-FJS0.64- 30	7.4 = 4.75/0.64	30	1.33	1.03	1.12	0.65	86.2

use. The sample mass was determined based on the control density and specimen volume, and the specimen was uniformly deposited into the test mold in three layers using the sand rain method, compacting each layer to the designated height.

2.4. Test procedure

Resonant column test: After loading the sample, a back pressure

controller applies a back pressure of $-20\,\mathrm{kPa}$ to maintain the stability of the sample. Measure the initial height and diameter of the test specimen using a vernier caliper, taking the average of three measurements, Input into the testing software. Sequentially install the drive device, displacement sensor, and pressure chamber, then zero the vertical displacement. Incrementally increase the confining pressure four times by adding 5 kPa each time and unloading the back pressure by 5 kPa each time to ensure specimen stability. Maintain the back pressure at 0,

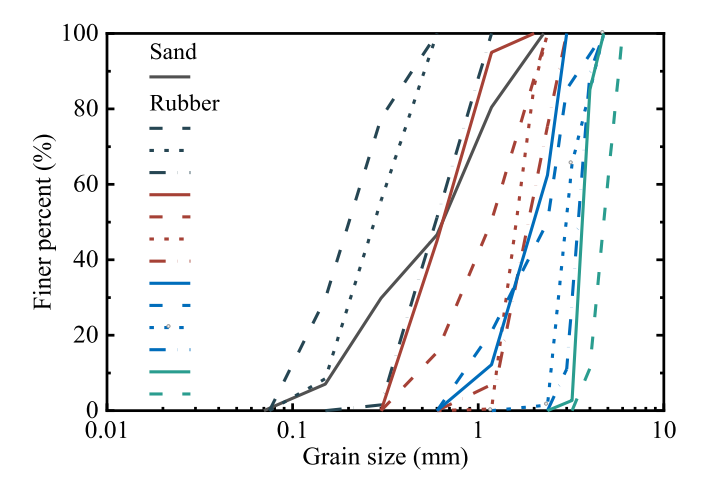


Fig. 2. Grain size distribution curves.

apply the desired confining pressure, and consolidate until the vertical displacement stabilizes (at least 1 h) [47]. After consolidation, a resonant column test was conducted. This test employs a frequency sweep resonant method to measure the peak acceleration and resonant frequency of the specimen, enabling the calculation of the dynamic shear modulus. Additionally, the damping ratio is determined based on the decay curve of free vibration.

Cyclic simple shear test: consolidate the specimen under different confining pressures (50 kPa, 100 kPa, 200 kPa) until the vertical displacement-time curve stabilizes. Maintain the vertical confining pressure constant during this phase. Perform horizontal cyclic shear testing using strain control. The strain amplitude ranges from 5×10^{-4} to 5×10^{-2} . Apply shear strain in increments, starting from small values and gradually increasing through 10 levels.

3. Results and discussion

3.1. Dynamic shear modulus (G_d)

3.1.1. Effect of PSR

Fig. 4 illustrates the influence of varying *PSR* on the dynamic shear modulus of RSM under different shear strain amplitudes. Among them, both the solid and dashed lines represent fitted curves, At small strain amplitudes, the dynamic shear modulus differs significantly across different *PSR* values, with changes reaching up to 3 to 4 times. Specifically, as the *PSR* increased from 0.3 to 5.8, the dynamic shear modulus initially decreased and then increased. Notably, when the *PSR* approaches 1.0, the $G_d \sim \gamma_d$ curve reaches its lowest point, indicating the minimum dynamic shear modulus. Although *PSR* continues to impact the dynamic shear modulus of RSM at larger strain amplitudes, this influence is less pronounced than at smaller strain amplitudes. At larger strain ranges, the differences in dynamic shear modulus between different *PSR* values are minimal, leading to closely clustered $G_d \sim \gamma_d$ curves. As the shear strain increases, the dynamic shear modulus remains relatively low for a *PSR* close to 1.0 across different curves.

3.1.2. Effect of confining pressure

Fig. 5 illustrates the fitting of experimental data within the small strain amplitude range using Eq (1). The resulting fitted curve is then extended to the large strain range for comparison with the measured data points at large strain amplitudes. The results show that while the fitted curve is consistent with the overall trend of the data points, it does not fully align with them. This indicates that the theoretical fitted curve cannot fully replace the measured data. Therefore, incorporating the measured data at large strain amplitudes is essential for accurately analyzing the dynamic behavior of RSM across a wide strain range, this helps to understand the dynamic behavior of RSM over a wide strain

range. Moreover, the consistency in trends between the fitted curve and the measured data points further suggests that the dynamic behavior of RSM exhibits continuity across different strain amplitudes.

Fig. 6 illustrates the effect of different confining pressures on the dynamic shear modulus of RSM under a constant *RC* across a wide strain range. Analysis reveals that the dynamic shear modulus of RSM increases significantly with the increase in confining pressure, and the impact of confining pressure decreases as *RC* increases. The effect of confining pressure on dynamic shear modulus is particularly significant at small strain amplitudes, suggesting it may be the primary factor driving changes in dynamic shear modulus. At the same time, confining pressure still affects the dynamic shear modulus at large strain amplitudes, albeit to a lesser extent than at small strain amplitudes. The results indicate that both confining pressure and *RC* cause non-linear changes in dynamic shear modulus, with varying degrees of influence under different conditions.

The influence of frequency should not be overlooked. Due to the significant differences in frequency between the resonant column test and the cyclic simple shear test, in this study, the frequency range used for the resonant column test was 10–100 Hz, whereas the frequency employed in the cyclic simple shear test apparatus was 1 Hz. Research has shown that variations in frequency have a substantial impact on the dynamic shear modulus of RSM. Specifically, as the frequency increases, the dynamic shear modulus tends to increase as well. Therefore, in practical applications, it is crucial to consider the effect of frequency on the performance of RSM.

3.1.3. Effect of RC

Fig. 7 illustrates the effect of varying *RC* on the dynamic shear modulus under constant confining pressure across a wide range of strain amplitudes. The analysis reveals a significant decrease in the dynamic shear modulus of RSM with increasing *RC*. As *RC* risen from 0 % to 25 %, the downward trend was particularly significant. However, as *RC* further increased from 25 % to 30 %, the rate of decline gradually slowed. Furthermore, noticeable differences in the downward trend were observed under different strain amplitudes. Specifically, *RC* had the most significant effect on the decrease in dynamic shear modulus under small strain amplitudes, indicating it is a key factor driving changes at this level of strain. At large strain amplitudes, although *RC* still affected the dynamic shear modulus, this impact was significantly weakened compared to small strain amplitudes.

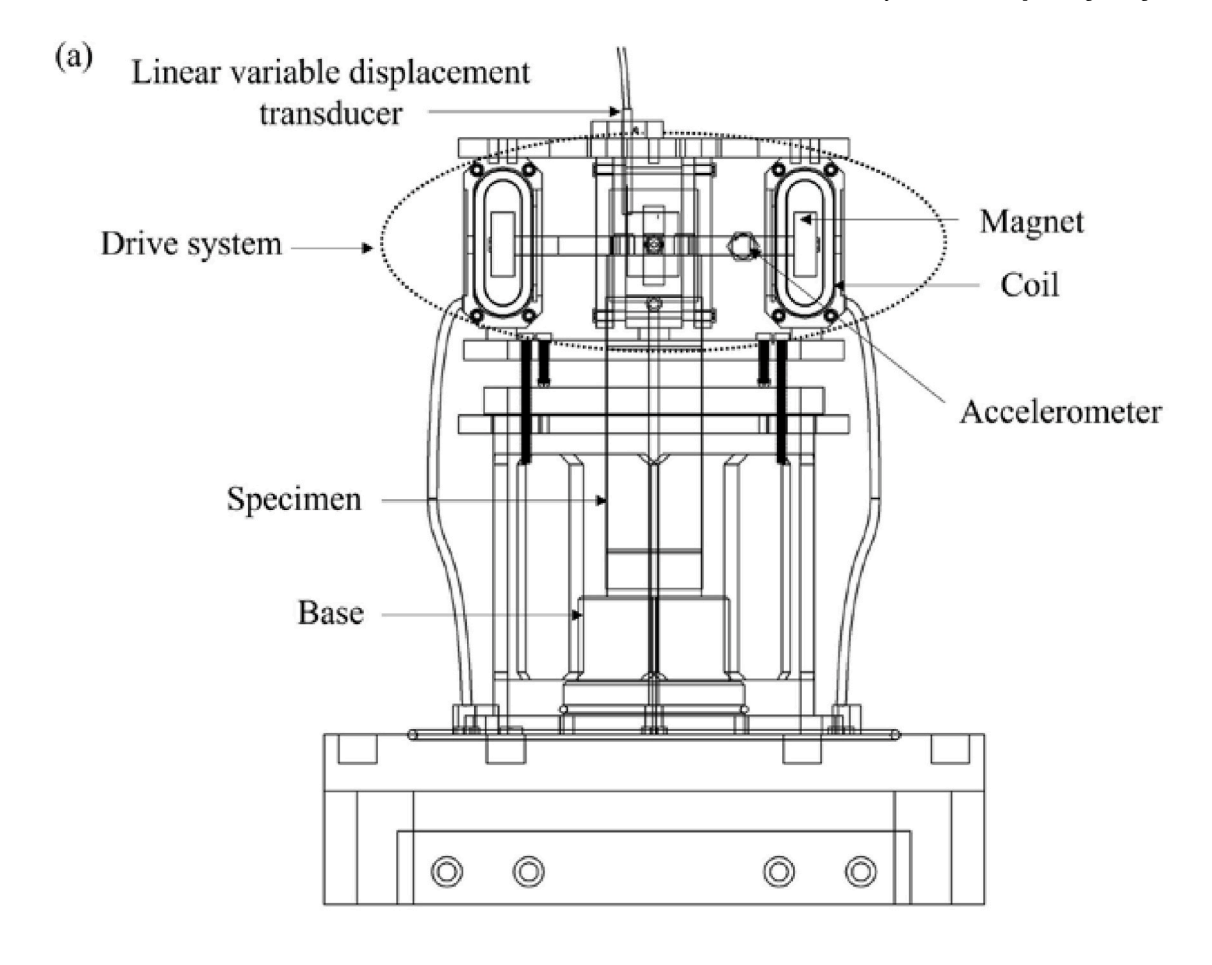
3.2. Maximum dynamic shear modulus

The maximum dynamic shear modulus is a crucial measure of soil dynamic characteristics and a necessary parameter for the dynamic response analysis of rock and soil. Using the classic Hardin and Drnevich formula to fit the $G_{\rm d} \sim \gamma_{\rm d}$ curve [48].

$$G_{\rm d} = \frac{G_{\rm dmax}}{1 + \left(\gamma_{\rm d} / \gamma_{\rm d.ref}\right)^a} \tag{1}$$

where $G_{\rm dmax}$ is the maximum dynamic shear modulus; $\gamma_{\rm d}$ is the dynamic shear strain amplitude; $G_{\rm d}$ is the dynamic shear modulus corresponding to the dynamic shear strain $\gamma_{\rm d}$, and $\gamma_{\rm d,ref}$ is the reference shear strain, for which the corresponding dynamic shear modulus is 0.5 $G_{\rm dmax}$ [49]. It can be observed that as $\gamma_{\rm d,ref}$ increases, the rate of decay of the dynamic shear modulus slows down. a is the modulus curve attenuation parameters.

The maximum dynamic shear modulus value shown in Fig. 8 is based on the fitting of experimental data using Fitting Eq (1), with the obtained value corresponding to the maximum stiffness at the minimum strain level (due to device limitations), Analysis found that the maximum dynamic shear modulus of RSM reaches the lowest point in the $G_{\rm dmax} \sim PSR$ curve when the PSR is close to 1.0 (with the exception when RC = 5



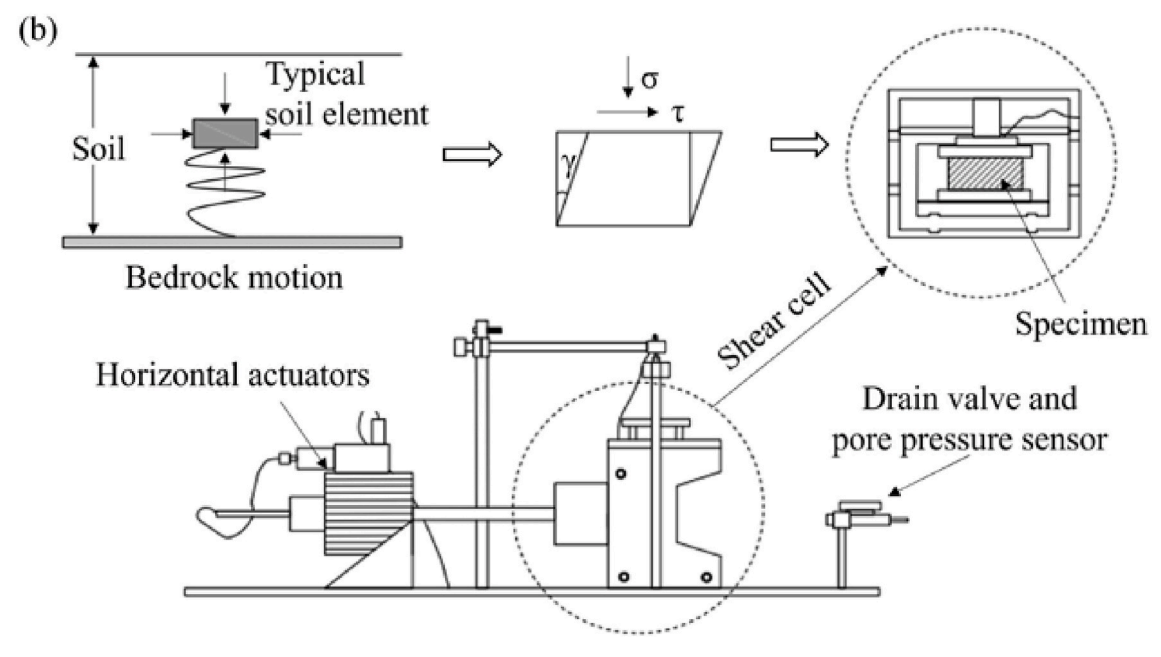


Fig. 3. Schematic diagram of test apparatus: (a) GDS resonant column testing system (b) Cyclic simple shear test system.

%). As the *PSR* increases from 0.3 to 5.8, the $G_{\rm dmax} \sim PSR$ curve of RSM varies with different *RC*. Specifically, at an *RC* of 5 %, the maximum dynamic shear modulus decreases slowly with increasing *PSR*. However, at an *RC* of 10 %–20 %, the maximum dynamic shear modulus first decreases and then increases, with a turning point near a *PSR* of 1.0.

When the RC increases to 25 %–30 % and the $PSR \leq 3$, the variation trend of $G_{\rm dmax}$ with PSR is similar to that when RC is in the range of 10 %–20 %. However, as the PSR continues to increase, there will be slight fluctuations in $G_{\rm dmax}$. Based on existing studies [18,50], the recommended RC of RSM is between 20 % and 30 %, However, some studies

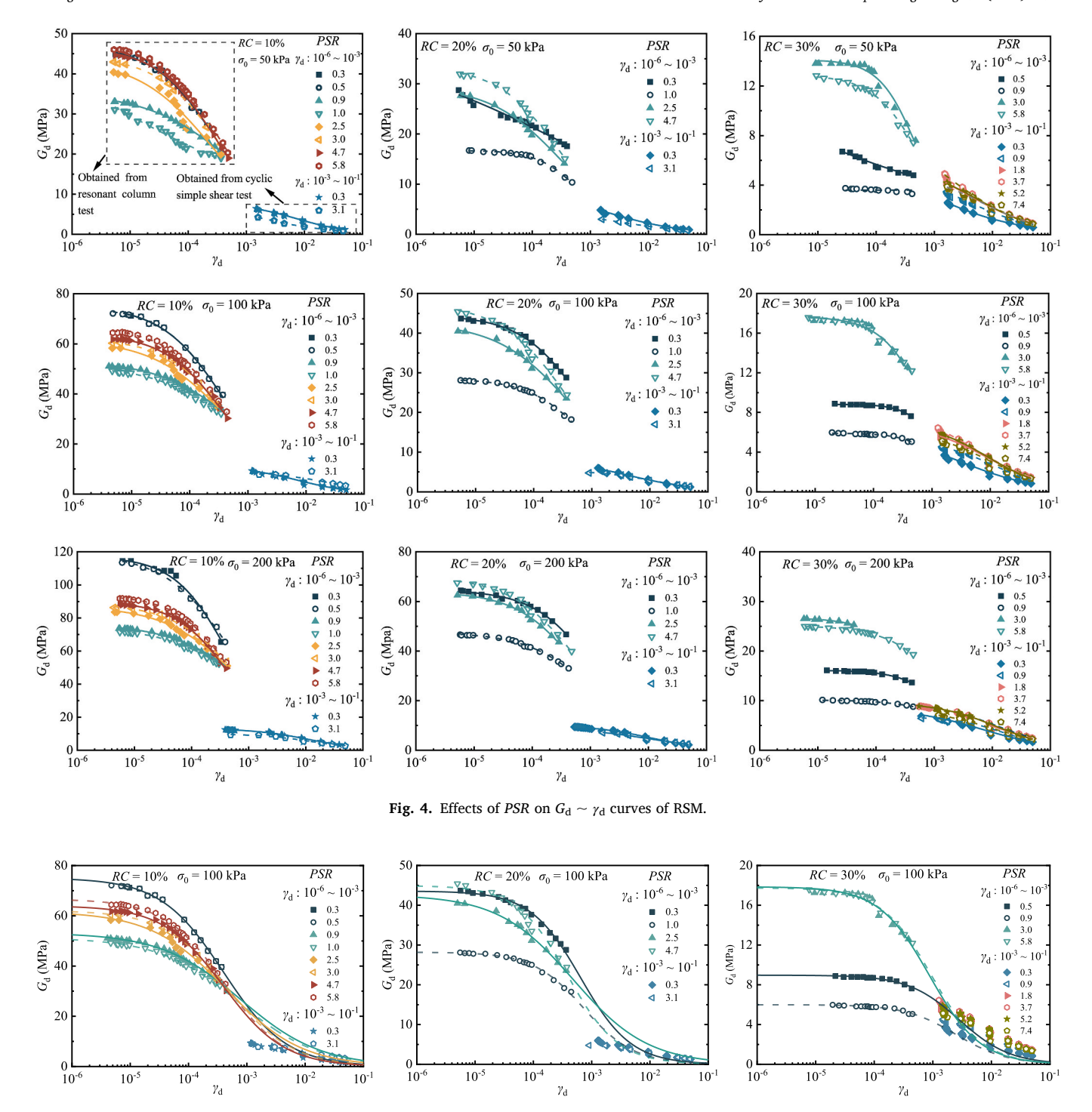


Fig. 5. The fitting $G_{\rm d} \sim \gamma_{\rm d}$ curve under small strain amplitude is compared with large strain data.

[51] have shown that an RC of less than 20 % can meet the requirements for shear stiffness in railroad subgrade engineering. An optimal PSR for RSM as seismic isolation material may be close to 1.0, making it suitable as a seismic buffer material. Under the same RC, $G_{\rm dmax} \sim PSR$ curves under different confining pressures are almost parallel. This indicates that changes in confining pressure will not affect the variation pattern of $G_{\rm dmax}$, while nonlinear changes in maximum dynamic shear modulus are mainly influenced by both RC and PSR.

In Fig. 9a, the variation of the maximum dynamic shear modulus of RSM with RC is analyzed when the PSR approaches 1.0. As RC increases from 0 % to 25 %, the maximum dynamic shear modulus of RSM decreases significantly. However, the rate of decline slows as RC increases

from 25 % to 30 %. Furthermore, confining pressure also significantly impacts the maximum dynamic shear modulus. Specifically, at low levels of RC (e.g., 5 %), an increase in confining pressure substantially raises the maximum dynamic shear modulus. However, as RC reaches higher levels (e.g., 25 %), the influence of confining pressure on the maximum dynamic shear modulus diminishes, indicating that increasing RC weakens its influence. A comparison of the experimental results from this study with Nakhaei et al. [25], shows consistent trends. Specifically, the maximum dynamic shear modulus decreases with an increase in RC and increases with an increase in confining pressure. Furthermore, the varying degrees of influence of RC and confining pressure on the maximum dynamic shear modulus of RSM align with our

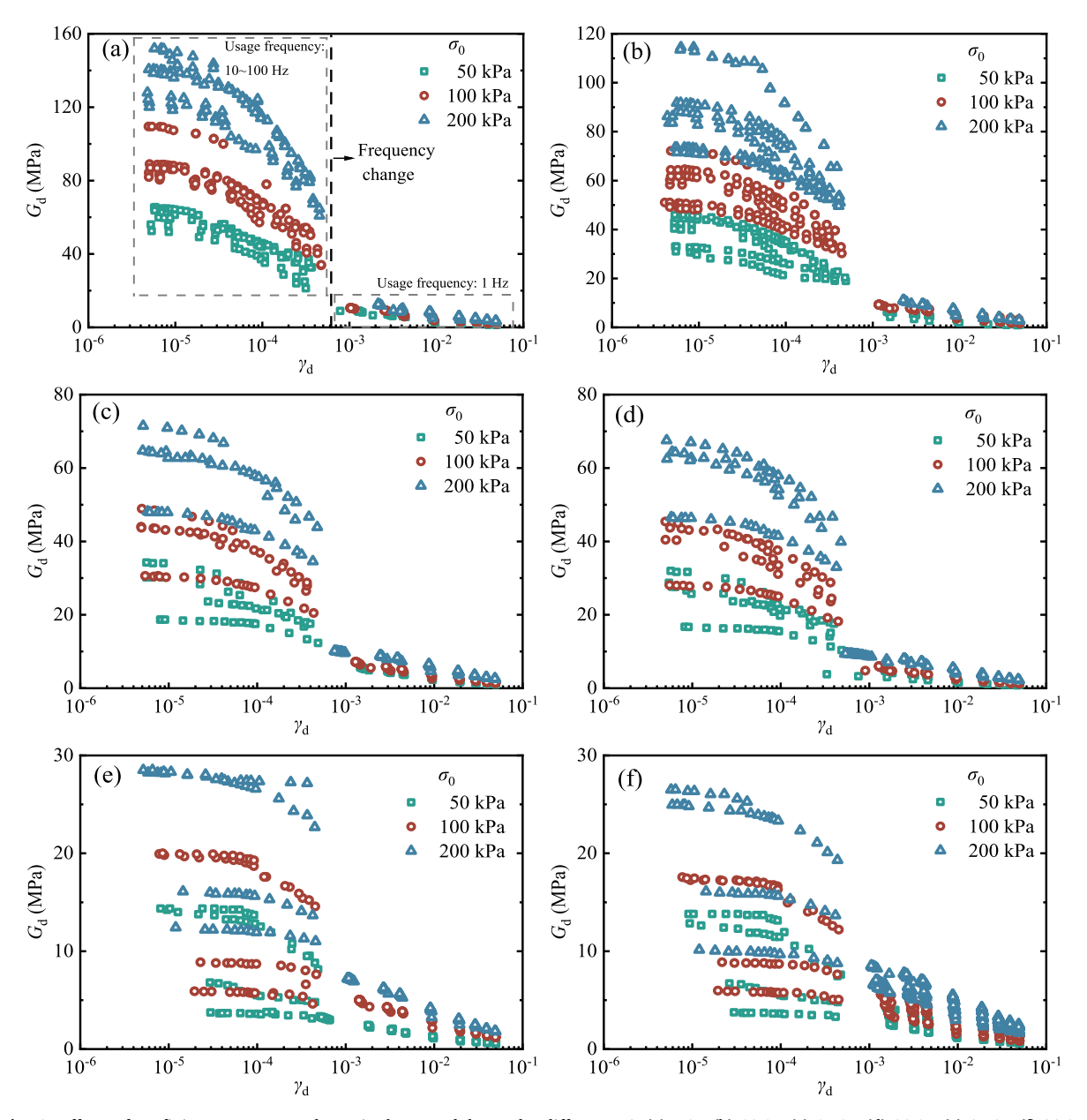


Fig. 6. Effects of confining pressures on dynamic shear modulus under different RC: (a) 5 %, (b) 10 %, (c) 15 %, (d) 20 %, (e) 25 %, (f) 30 %.

conclusion

In comparison with the findings of Lee et al. [21] regarding *PSR* (Fig. 9c), analogous traits are noted. Specifically, for *PSR* less than 1.0, the maximum dynamic shear modulus of RSM diminishes as *PSR* increases. When *PSR* approaches 1.0, the maximum dynamic shear modulus of RSM reaches its lowest point. As *PSR* exceeds 1.0 and continues to increase, the maximum dynamic shear modulus of RSM shows a significant upward trend. These shared characteristics substantiate the precision and reliability of the presented test data.

3.3. $G_d/G_{dmax} \sim \gamma_d$ curves

Fig. 10 shows the $G_{\rm d}/G_{\rm dmax}\sim \gamma_{\rm d}$ curves were compared under different confining pressure, PSR, and RC conditions to analyze the influence of various factors on the attenuation curve, The results indicate that increasing the confining pressure significantly retards the decay trend of the $G_{\rm d}/G_{\rm dmax}\sim \gamma_{\rm d}$ curves and enhances its linear characteristics. When the RC is 5 %, the normalized curve closely resembles that of pure sand, with minimal change in decay rate. However, at an RC of 20 %,

there is a significant decrease in the decay rate, suggesting that RSM with high RC exhibits better elasticity. Furthermore, comparing normalized curves for different PSR values reveals that when PSR exceeds or falls below 1.0, there is a notable increase in decay rate for the $G_{\rm d}/G_{\rm dmax} \sim \gamma_{\rm d}$ curves; conversely, when PSR approaches 1.0, the decay rate becomes relatively gentle.

3.4. Damping ratio (D)

The Darendeli-Stokoe model [49] is used to fit the test results of the damping characteristics of RSM, as shown in Eqs. (2)–(7).

$$D = b \left(\frac{G_{\rm d}}{G_{\rm dmax}}\right)^{0.1} D_{\rm masing} + D_{\rm min} \tag{2}$$

$$D_{\text{masing}} = c_1 D_{\text{masing}, a=1.0} + c_2 D_{\text{masing}, a=1.0}^2 + c_3 D_{\text{masing}, a=1.0}^3$$
 (3)

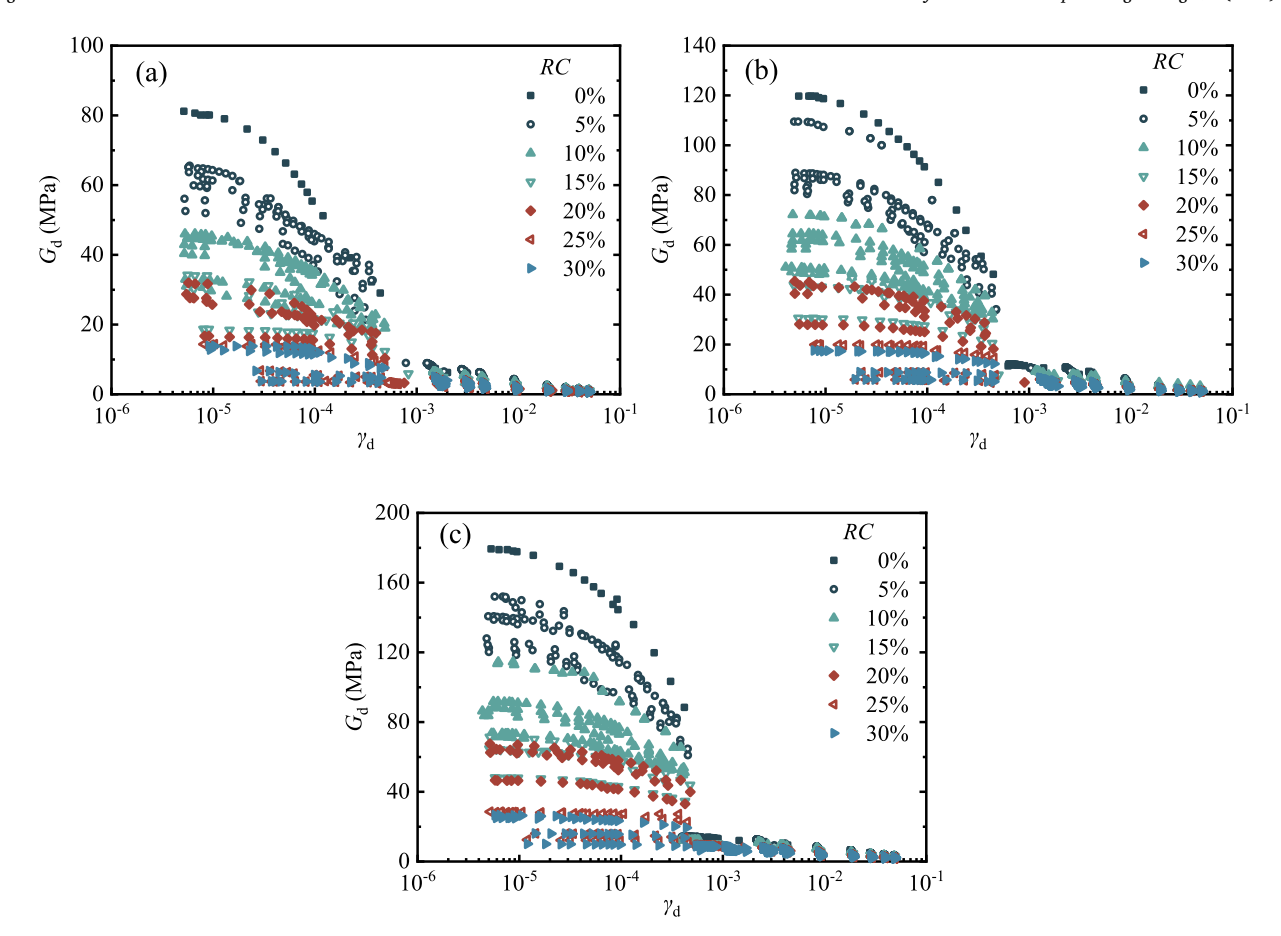


Fig. 7. Effect of RC on dynamic shear modulus under different confining pressures: (a) 50 kPa,(b) 100 kPa,(c): 200 kPa.

$$D_{\text{masing,a=1.0}}(\%) = \frac{100}{\pi} \left[4 \frac{\gamma_{\text{d}} - \gamma_{\text{d,ref}} \ln \left(\frac{\gamma_{\text{d}} + \gamma_{\text{d,ref}}}{\gamma_{\text{d,ref}}} \right)}{\frac{\gamma_{\text{d}}^2}{\gamma_{\text{d}} + \gamma_{\text{d,ref}}}} - 2 \right]$$
(4)

$$c_1 = -1.1143a^2 + 1.8618a + 0.2523 \tag{5}$$

$$c_2 = 0.0805a^2 - 0.0710a + 0.0095 \tag{6}$$

$$c_3 = -0.0005a^2 + 0.0002a + 0.0003 \tag{7}$$

where D is the damping ratio, $D_{\rm masing}$ indicates the expected damping ratio of the Masing hysteresis criterion, and $D_{\rm min}$ denotes small strain damping ratio, b is the damping ratio curve parameter. (See Eq. (1) for an explanation of part of the terms)

The Darendeli-Stokoe dynamic characteristic equation is based on hundreds of conventional soil dynamic characteristic test results. This model improves upon the Hardin-Drnevich model [48] by correcting the shortcomings of the Masing criterion, which fails to accurately simulate soil damping ratios. As a result, it can be widely applied in the simulation of dynamic shear modulus and damping ratios for conventional soils. Due to the device's limitations, this study determined the $G_{\rm dmax}$ and $D_{\rm min}$ values of RSM through inverse analysis. The specific fitted parameter values are listed in Table 5.

3.4.1. Effect of PSR

Fig. 11 illustrates the effect of different *PSRs* on the damping ratio of RSM under wide strain. The impact of *PSR* on the damping ratio is relatively complex with the various $D \sim \gamma_{\rm d}$ curves closely intertwined. Specifically, within the small strain amplitude range, the influence of

PSRs on the damping ratio shows that as the *PSR* increases, the corresponding damping ratio first decreases and then increases. The damping ratio reaches its minimum value when the *PSR* approaches 1.0. In contrast, within the large strain amplitude range, although the damping ratio remains low when the *PSR* is close to 1.0, it exhibits a complex interwoven relationship with the damping ratios corresponding to other *PSRs*. This behavior is remarkably different from the systematic variations observed in the influence of *PSRs* on the damping ratio within the small strain amplitude range, suggesting that alterations in the shear strain amplitude range also affect the influence of *PSR* on the damping ratio

In Fig. 12, under constant RC and confining pressure, representative PSRs selected at small and large strain amplitudes were used to plot the $G_{\rm d}/G_{\rm dmax} \sim D$ curves for each sample. The $G_{\rm d}/G_{\rm dmax} \sim D$ curves for different PSRs exhibited varying slopes at different strain amplitudes: at larger strain amplitudes, the linear relationship was more pronounced, with the decay rate regions between different PSRs being similar. In contrast, at smaller strain amplitudes, the curves showed greater disparity, indicating that larger PSRs resulted in faster decay rates. This further confirms that changes in shear strain amplitude significantly influence the extent to which variations in PSR affect the damping ratio.

3.4.2. Effect of confining pressure

Fig. 13 illustrates the effect of different confining pressures on the damping ratio of RSM over a wide strain range with constant *RC*. The damping ratio of RSM is significantly influenced by confining pressure, exhibiting regular patterns of variation. Throughout the entire strain range, increasing confining pressure results in a decrease in the damping ratio. However, the effect of confining pressure on the damping ratio varies with different shear strain amplitudes. At small strain amplitudes, an increase in confining pressure also lowers the damping ratio, but the

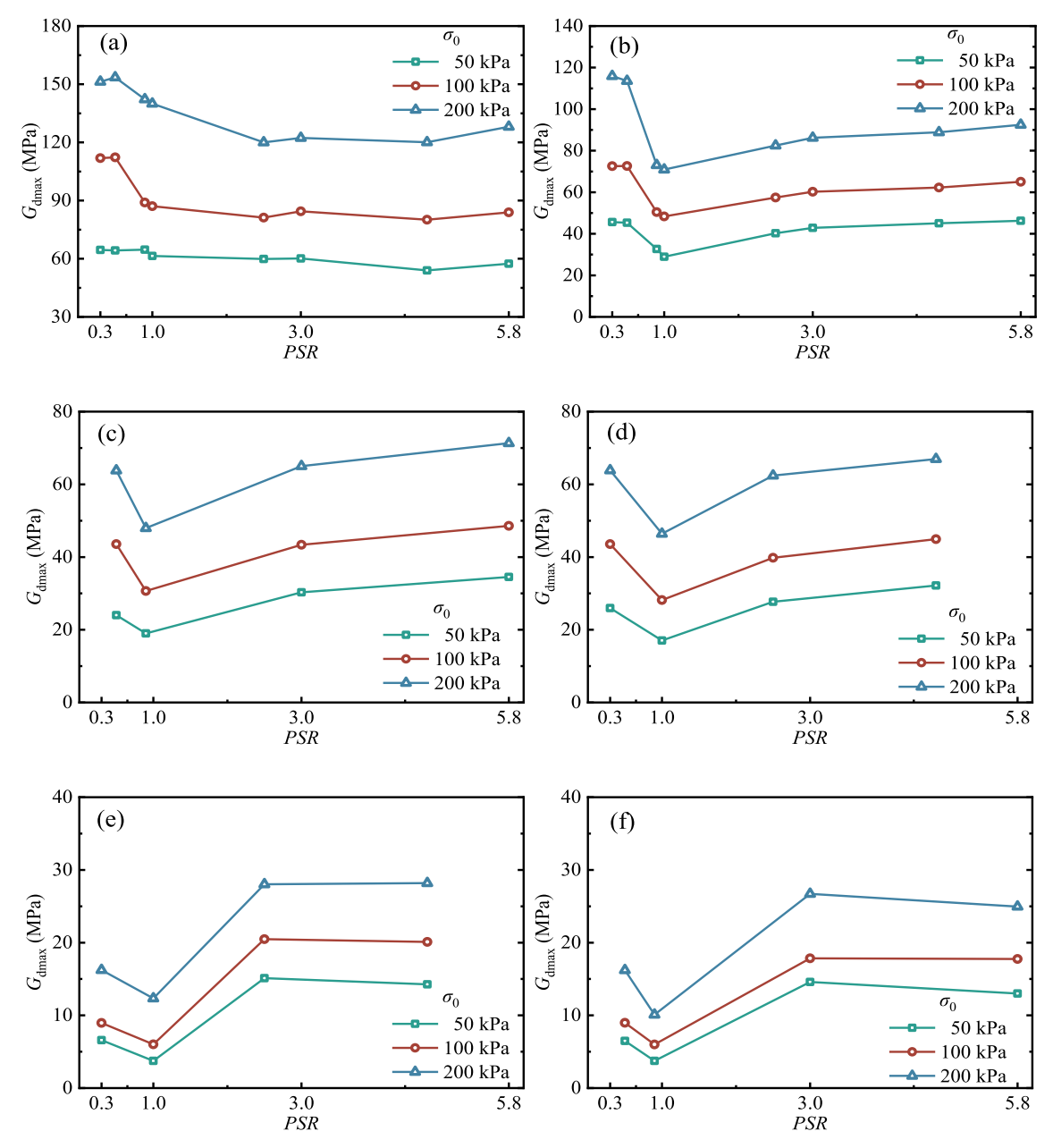


Fig. 8. The variation of maximum dynamic shear modulus of RSM with PSR under different RC:(a) 5 %, (b) 10 %, (c) 15 %, (d) 20 %, (e) 25 %, (f) 30 %.

decrease is not as pronounced as that observed under large strain conditions. As shear strain increases, the influence of confining pressure on the damping ratio becomes more significant, and this trend remains consistent across different *RC* levels. This indicates that changes in both confining pressure and shear strain amplitude jointly affect the damping ratio.

3.4.3. Effect of RC

The damping ratio values of RSM with different *PSRs* are combined according to the *RC*, and the fitting curves are obtained through Eqs. (2)–(7). Fig. 14 illustrates the variation of the damping ratio as a function of both *RC* and strain amplitude. At small shear strains, the $D \sim \gamma_{\rm d}$ curve of pure sand typically falls at the lower end, while the curve for mixtures with higher *RC* appears at the upper end. At this strain amplitude, the damping ratio of RSM increases with increasing *RC*. As shear strain and confining pressure increase, RSM with varying *RC* exhibits different damping characteristics. The damping ratio growth of RSM with higher *RC* (e.g., 25 %, 30 %) progressively slows down.

Overall, the damping ratio of RSM with varying *RC* increases with the increase in shear strain. Notably, the most significant rise in the damping ratio occurs between shear strains of 10^{-2} to 10^{-1} .

3.4.4. Damping ratio comparison

Fig. 15 illustrates the damping ratio of RSM with varying RC under a confining pressure of 100 kPa, providing a comparative analysis against similar studies. The findings indicate that the variation trend of the damping ratios in this research aligns closely with those observed in previous studies. Notably, within the range of $\gamma_d = 10^{-6} \sim 10^{-3}$, the damping ratios show a relatively tight distribution. In contrast, within the range of $\gamma_d = 10^{-3} \sim 10^\circ$, the damping ratios of the RSM exhibit a more pronounced degree of dispersion. Overall, the damping ratio of the RSM presents a discernible distribution pattern across a wide strain range. The variation in shear strain amplitude emerges as a crucial factor: as the shear strain amplitude increases, the damping ratio also rises, demonstrating a consistent and systematic trend in its growth.

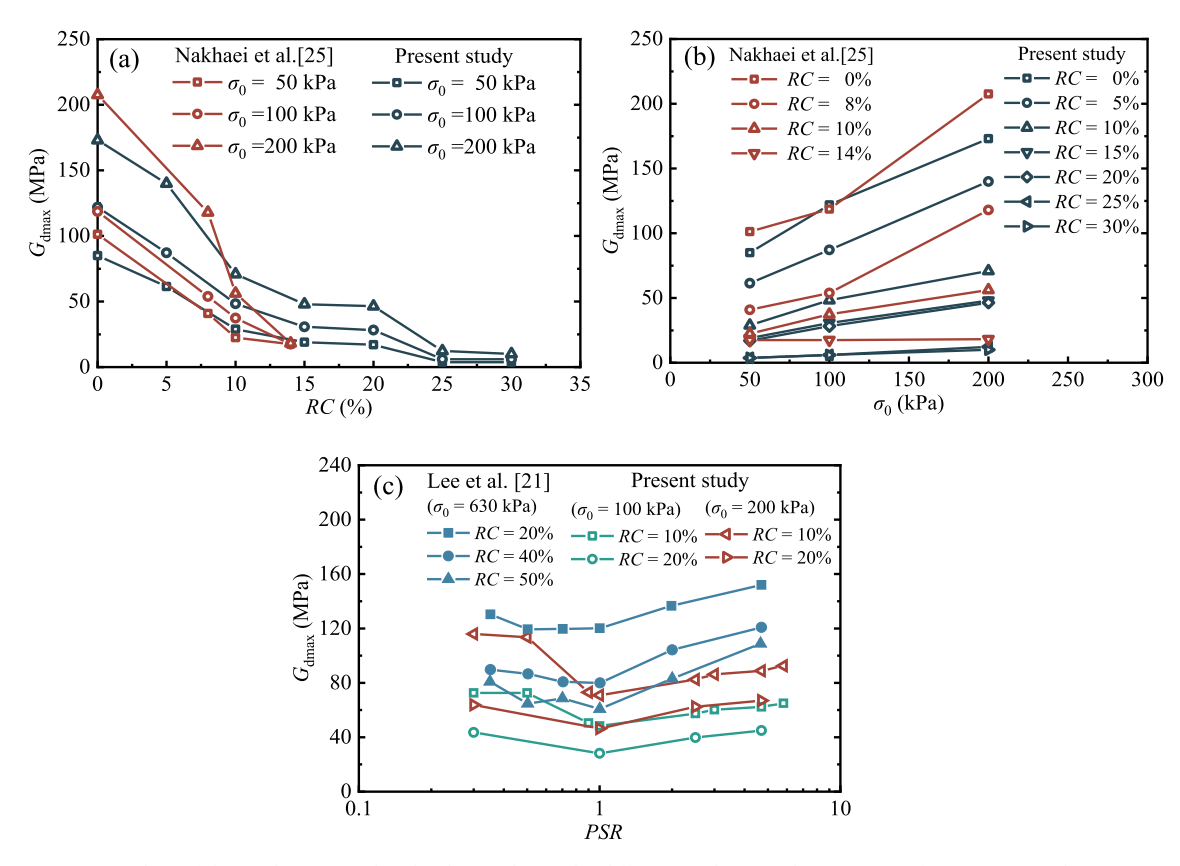


Fig. 9. G_{dmax} values of this study compared with other studies under different working conditions: (a) confining pressure, (b) RC, (c) PSR.

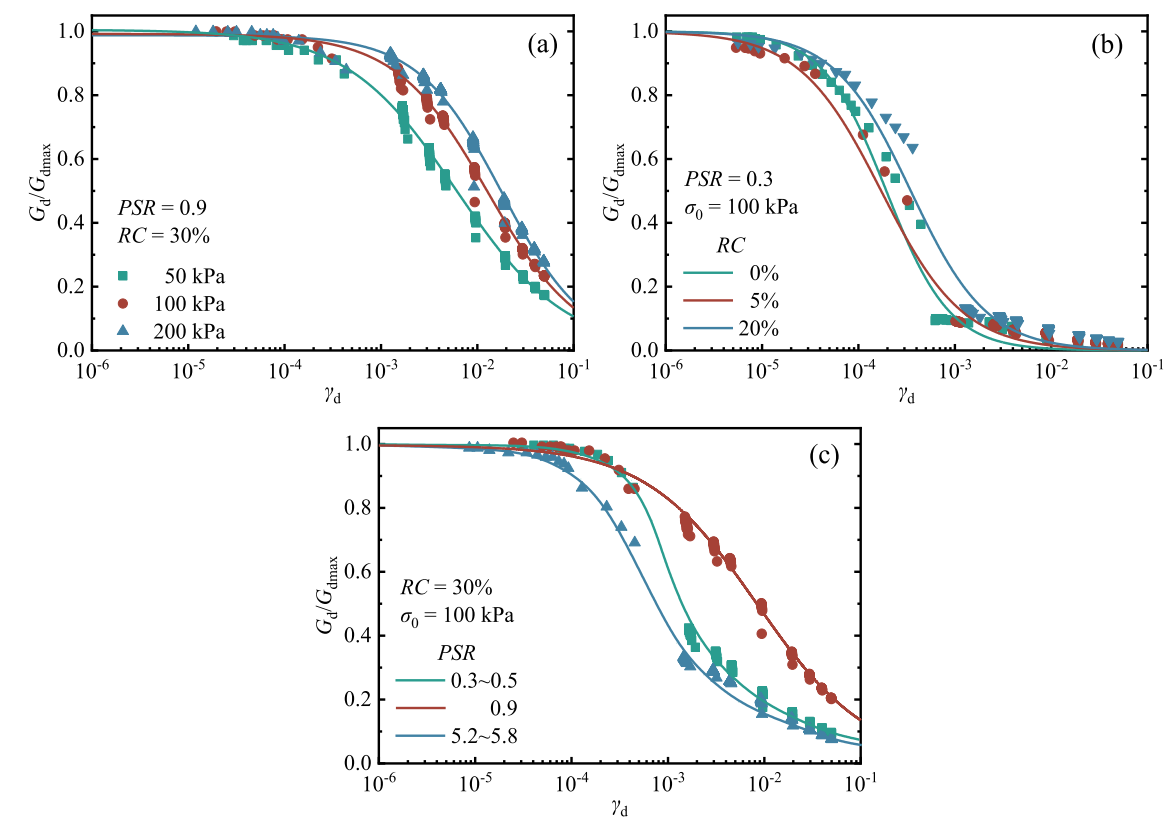


Fig. 10. $G_{\rm d}/G_{\rm dmax} \sim \gamma_{\rm d}$ curves of under different working conditions: (a) confining pressure, (b) RC, (c) PSR.

Table 5Parameter values for RSM fitting curves in the resonant column tests.

PSR	RC (%)	G _{dmax} (MPa)	a	7d,ref	b	D _{min} (%)
_	0	123.0	0.965	0.0003	0.057	0.475
0.3	5	111.8	0.952	0.0003	0.044	0.805
	10	72.6	0.803	0.0004	0.167	1.442
	20	43.6	0.815	0.0007	0.088	1.717
	25	9.0	1.553	0.0015	0.127	1.847
0.5	5	112.3	0.961	0.0003	0.055	0.649
	10	72.6	0.820	0.0004	0.168	1.429
	15	43.6	0.822	0.0007	0.084	1.683
	30	9.0	1.691	0.0013	0.122	1.856
0.9	5	89.0	0.668	0.0004	0.111	0.497
	10	50.5	0.633	0.0008	0.077	0.702
	15	30.7	0.894	0.0009	0.071	0.820
	30	6.0	1.441	0.0015	0.009	1.561
1.0	5	87.1	0.745	0.0004	0.092	0.503
	10	48.4	0.634	0.0007	0.101	0.773
	20	28.2	0.899	0.0008	0.073	0.889
	25	6.0	1.804	0.0006	0.049	1.681
2.5	5	81.2	0.782	0.0003	0.092	0.595
	10	57.5	0.670	0.0004	0.065	1.101
	20	39.8	0.676	0.0005	0.066	1.426
	25	20.5	1.091	0.0010	0.117	1.846
3.0	5	84.4	0.849	0.0004	0.089	0.602
	10	60.2	0.791	0.0005	0.064	1.082
	15	43.4	0.690	0.0006	0.070	1.489
	30	17.9	1.133	0.0008	0.118	1.842
4.7	5	80.1	0.774	0.0003	0.053	0.817
	10	62.3	0.831	0.0004	0.079	1.805
	20	44.9	0.751	0.0004	0.064	1.026
	25	20.1	1.016	0.0011	0.107	1.552
5.8	5	83.9	0.884	0.0003	0.089	0.664
	10	65.0	0.840	0.0004	0.085	1.818
	15	48.6	0.816	0.0005	0.065	1.076
	30	17.8	1.063	0.0009	0.104	1.481

3.5. Discussion on prevailing mechanism

Rubber particles in the mixture exhibit low modulus and high deformability, while sand particles are approximately rigid bodies but may experience angular breakage. Shear deformation in RSM leads to relative positional movement between rubber and sand particles. The incorporation of rubber particles with good elastic deformation capacity makes relative displacement between particles easier, decreasing the dynamic shear modulus with increasing RC. At small strain amplitudes, rubber particles promote inter-particle displacement through elastic deformation, and increase the damping ratio through rubber particle deformation. Consequently, a higher RC results in a higher damping ratio of RSM at small strain amplitudes. At large strain amplitudes, the relative displacement between particles becomes more pronounced. In RSM with lower RC (e.g., 10 %) and pure sand, direct shear misalignment between sand particles may cause angular breakage, consuming energy. Conversely, in RSM with higher RC, rubber particles reduce direct contact between sand particles, decreasing angular breakage and energy consumption. Therefore, at large strain amplitudes, the damping ratio of RSM exhibits a more complex variation trend as a function of RC.

The influence of confining pressure on the dynamic properties of RSM can be analyzed from two aspects: Both rubber and sand particles in RSM are discrete materials, and their dynamic properties depend on sand particles and rubber particle's interparticle friction and interlocking. Among them, the impact of interparticle friction and interlocking force on its dynamic properties is significant. Increasing confining pressure decreases the porosity of RSM, resulting in a more dense particle arrangement, increased contact area between particles, and tighter interparticle friction and interlocking. Consequently, the shear deformation resistance (i.e., shear modulus) of RSM is enhanced, while the damping ratio is reduced.

The impact of PSR on the dynamic performance of RSM is primarily influenced by the three main types of contact within the mixture: sand-

sand contact, rubber-sand contact, and rubber-rubber contact. The variations in mechanical performance are attributed to the alterations in the force chain distribution, composed of these three types of contacts. Both *RC* and *PSR* can modify the distribution and contact states of rubber and sand particles, thereby exerting a coupled effect on the dynamic performance of RSM.

As the RC increases, the proportion of rubber within the mixture rises. When the PSR is significantly less than 1.0, the distribution of the rubber component becomes dispersed, with a considerable portion of the small rubber particles filling the voids between sand particles, thus not fully contributing to the overall force transfer. This mitigates the reduction in the mixture's deformation resistance, maintaining a relatively high dynamic shear modulus. When the PSR approaches 1.0, the sizes of rubber particles become comparable to the sand particles, leading to optimal contact between the two. In this state, the original sand-sand contact in the force chains is largely replaced by sand-rubber contact, resulting in the dynamic shear modulus reaching its lowest value. As the PSR exceeds 1.0 and continues to increase, the rubber component distribution consolidates, forming a few larger rubber particles suspended within the sand matrix. Due to the incompressibility of sand particles, these large rubber particles are surrounded by sand particles. They cannot be embedded, creating an arching effect that allows force chains to bypass them and continue through sand-sand contact. This explains the observed recovery in dynamic shear modulus when the PSR exceeds 0.9. The larger the PSR, the more concentrated the rubber component becomes, reducing the number of "incompressible cavities" that force chains must circumvent, leading to a more pronounced recovery in dynamic shear modulus. However, if the RC is sufficiently high, continuous adjacent cavities may form, weakening the lateral confinement of the arching effect on force chains and thereby allowing rubber particles to participate in force chain transmission. This explains the experimental observation that the dynamic shear modulus of RSM decreases again when the PSR increases from 3.0 to 5.8 at an RC of 30 %.

4. Conclusions

This study employed resonant column tests and cyclic simple shear tests to thoroughly examine the wide-strain dynamic characteristics of rubber-sand mixtures (RSM). The findings provide critical insights into the effects of particle size ratio (*PSR*), rubber content (*RC*), and confining pressure on the nonlinear dynamic shear modulus and damping ratio of RSM under a wide range of strain amplitudes ($\gamma_d = 10^{-6} \sim 10^{-1}$). The main conclusions are summarized as follows:

- (1) Over a wide strain range, the *PSR* significantly affects the dynamic shear modulus of RSM. At low strain amplitudes, there are marked differences in dynamic shear modulus across varying *PSR*s, with variations reaching up to 3–4 fold. When the *PSR* approaches 1, the dynamic shear modulus values are generally lower. Furthermore, as the *RC* increases, the dynamic shear modulus gradually decreases, particularly with a notable decline when the *RC* rises from 0 % to 25 %. However, when *RC* is further increased to 30 %, the rate of decrease in modulus significantly slows down. Additionally, an increase in confining pressure enhances the dynamic shear modulus of RSM, but this strengthening effect diminishes as the *RC* increases.
- (2) Over a wide strain range, the damping ratio of RSM exhibits a trend of initially decreasing and then increasing with changes in the *PSR*, with a critical point occurring when the *PSR* approaches 1. This phenomenon is especially pronounced at low strain ranges. As *RC* increases, the damping ratio gradually rises within the small strain amplitude range, while it displays complex interwoven variations in the large strain amplitude range. Moreover, an increase in confining pressure leads to a decrease in

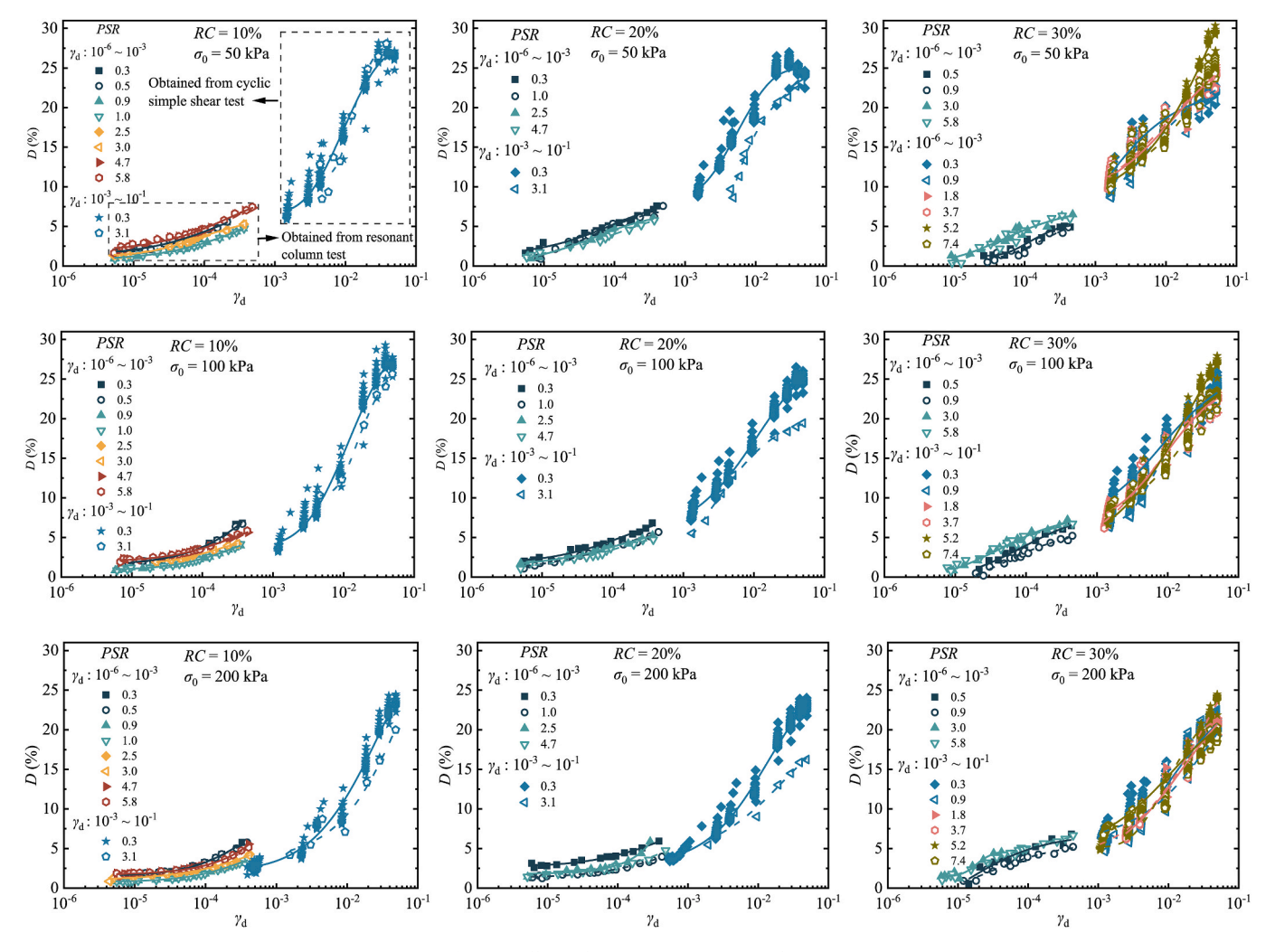


Fig. 11. Effects of PSR on D $\sim \gamma_d$ curves of RSM.

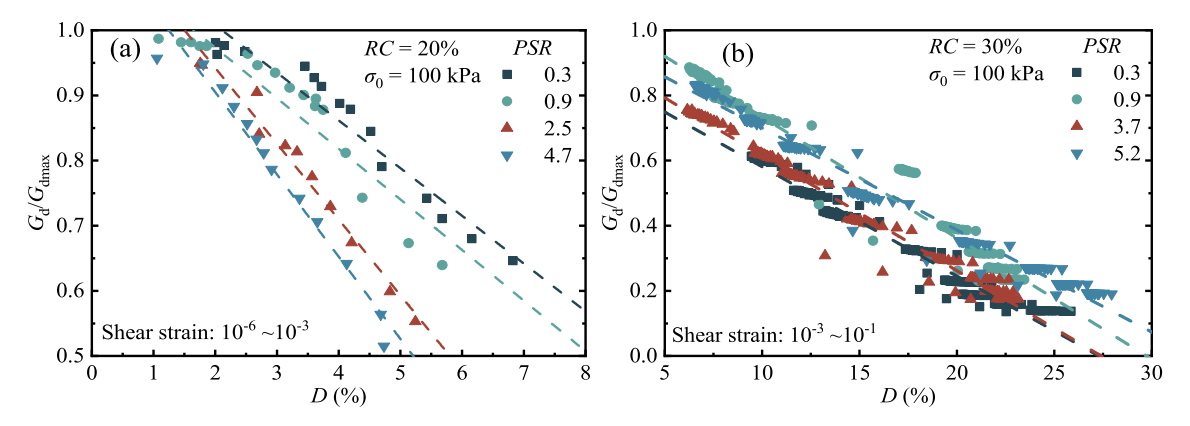


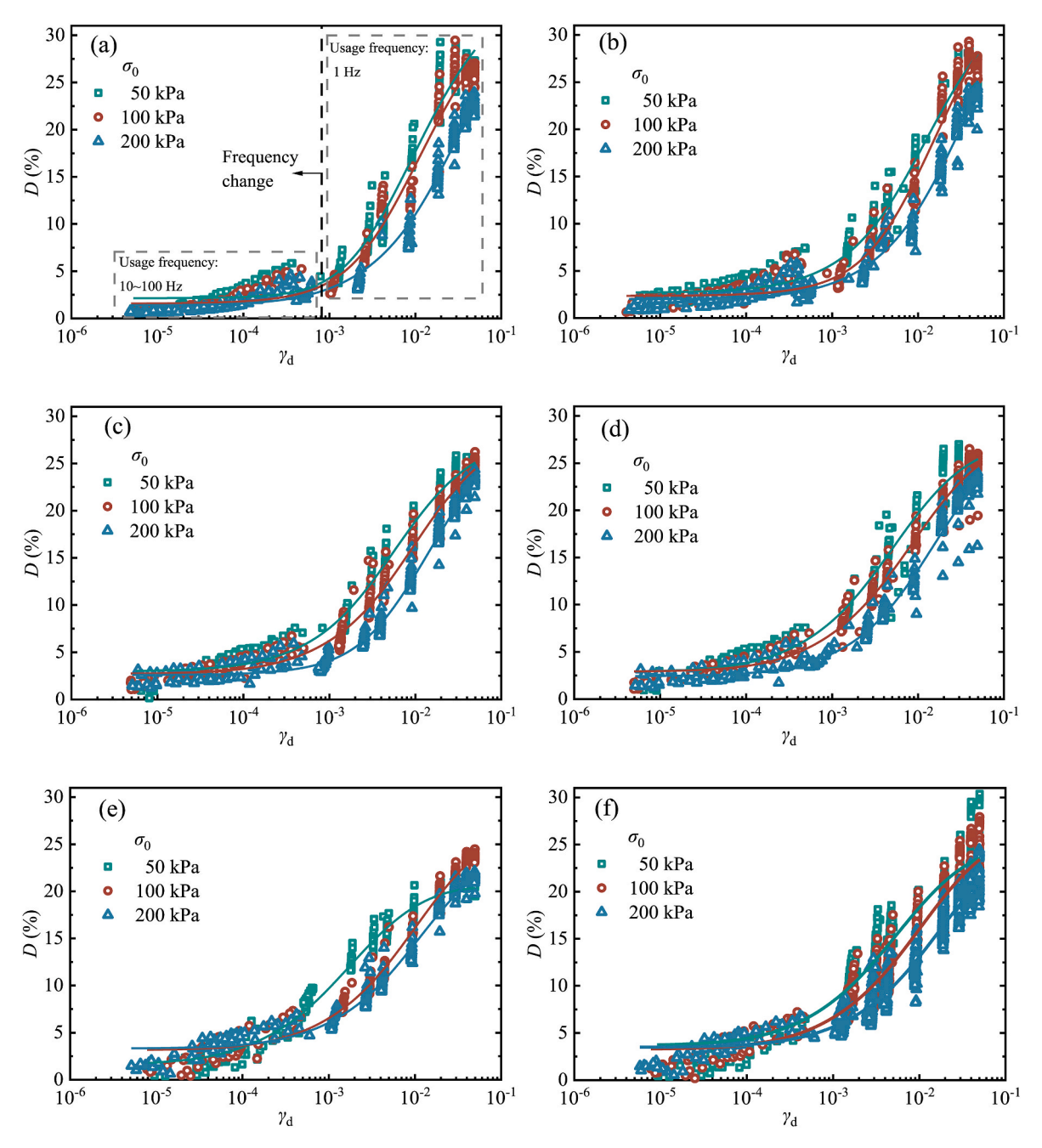
Fig. 12. $G_{\rm d}/G_{\rm dmax}\sim D$ curves of different PSR under different tests: (a) Resonant column tests; (b) Cyclic simple shear tests.

the damping ratio of RSM, a trend that remains consistent across the entire wide strain range.

(3) Although various factors can influence the dynamic shear modulus and damping ratio of RSM, the overall trend in dynamic characteristics remains consistent across a wide strain range. This suggests that RSM, as a type of energy-dissipating material, possesses relatively stable dynamic performance over a wide strain range.

CRediT authorship contribution statement

Wei Liang: Writing – original draft, Methodology, Investigation, Formal analysis, Conceptualization. Mengtao Wu: Writing – original draft, Resources, Investigation, Data curation, Conceptualization. Fangcheng Liu: Writing – review & editing, Supervision, Resources, Funding acquisition, Formal analysis, Conceptualization. Kai Zheng: Visualization, Investigation, Data curation. Jun Yang: Supervision, Resources. Jie He: Visualization, Resources.



 $\textbf{Fig. 13.} \ \, \textbf{Effects of confining pressures on the damping ratio under different RC: (a) 5 \%, (b) 10 \%, (c) 15 \%, (d) 20 \%, (e) 25 \%, (f) 30 \%.$

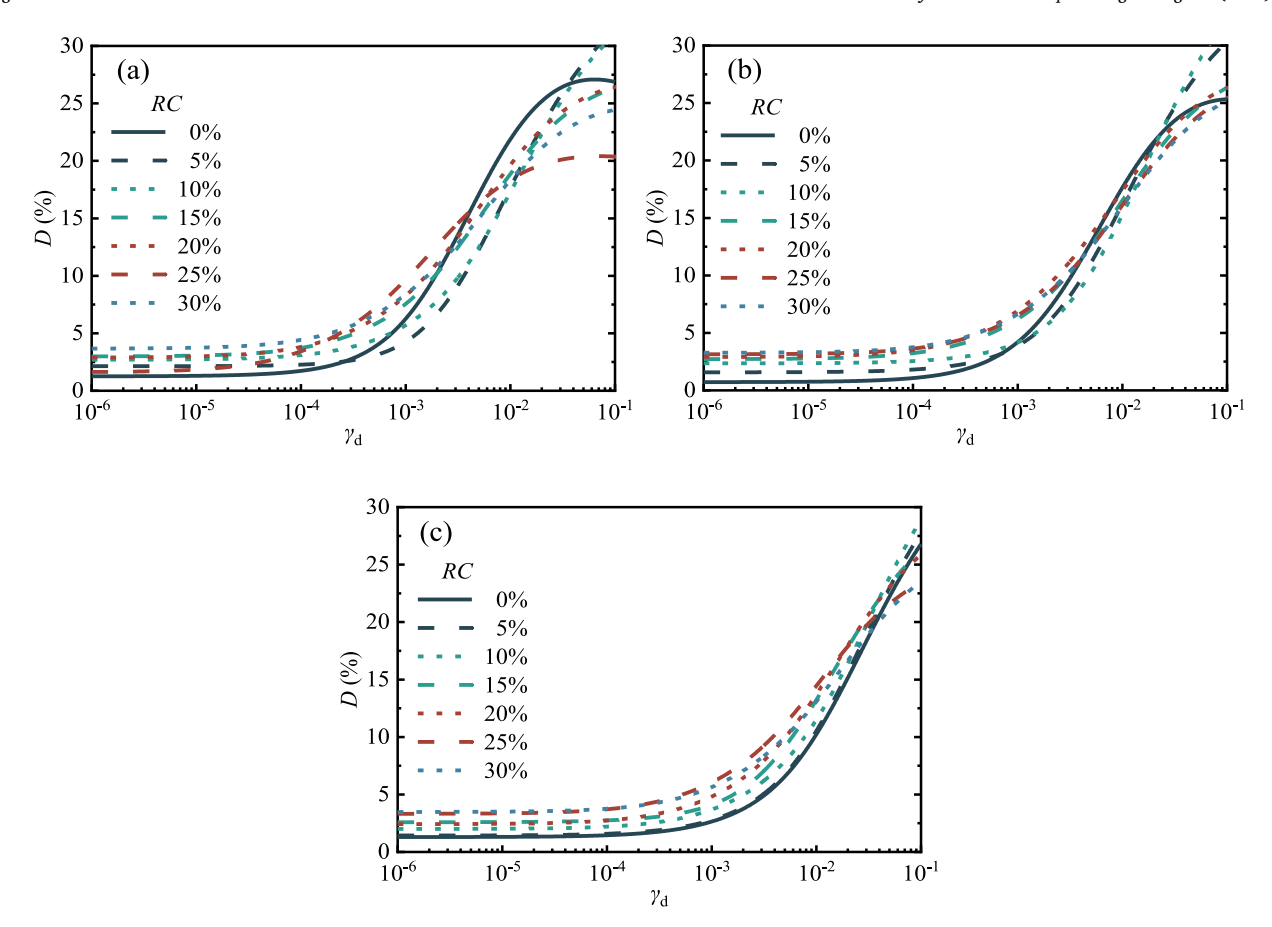


Fig. 14. Effects of RC on the damping ratio under different confining pressure: (a) 50 kPa, (b) 100 kPa, (c) 200 kPa.

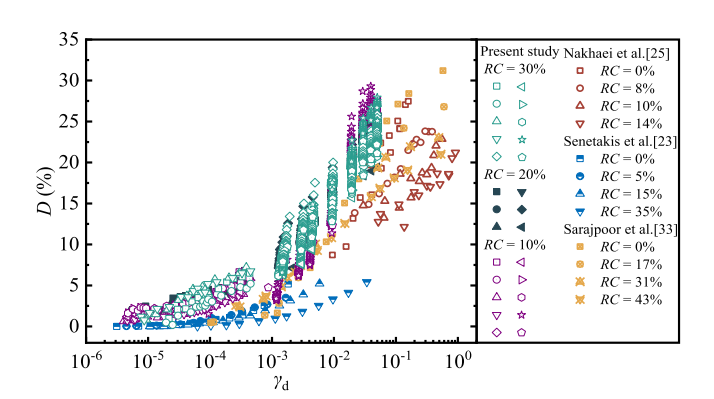


Fig. 15. Damping ratio comparison: confining pressure of 100 kPa.

Declaration of competing interest

The authors declare that they have no known competing financial interests or personal relationships that could have appeared to influence the work reported in this paper.

Acknowledgments

This research is sponsored by the Natural Science Foundation of Hunan Province under Grant No. 2025JJ50235, the Natural Science Foundation of China under Grant No. 52308500, the Education Department Project of Hunan Province of China under Grant No. 23B0556, the Postdoctoral Fellowship Program of CPSF under Grant No. GZB20230487, the China Postdoctoral Science Foundation under Grant

No. 2023M732480, the Sichuan Science and Technology Program under Grant No. 2024NSFSC0912, the Scientific Research and Innovation Foundation of Hunan University of Technology under Grant No. LXBZZ2419, and the Sichuan University Interdisciplinary Innovation Fund.

Data availability

Data will be made available on request.

References

- Duda A, Kida M, Ziembowicz S, Koszelnik P. Application of material from used car tyres in geotechnics—an environmental impact analysis. PeerJ 2020;8:e9546. https://doi.org/10.7717/peerj.9546.
- [2] Liu HS, Mead JL, Stacer RG. Environmental effects of recycled rubber in light-fill applications. Rubber Chem Technol 2000;73(3):551–64. https://doi.org/10.5254/ 1.3547605
- [3] Zheng K, Wu M, Yang J, Liang W, He J, Liu F. Time-dependent dynamic behavior of rubber-sand mixtures at small to medium strains: influence of rubber thermal aging and loading history. Constr Build Mater 2025;465:140218. https://doi.org/ 10.1016/j.conbuildmat.2025.140218.
- [4] Liang W, Wu M, Liu F, Zheng K, He J. Small-strain dynamic characteristics of multilayered rubber-sand composites. Geosynth Int 2025:1–16. https://doi.org/ 10.1680/jgein.24.00140.
- [5] Finney B, Chandler ZH, Bruce JL, Apple B. Properties of tire derived aggregate for civil engineering applications. California Dept. of Resources Recycling and Recovery (CalRecycle). Sacramento: Humbolt State Univ.; 2013.
- [6] WBCSD. World business council for sustainable development. Managing end-of-life tires (ELTs). Geneva, Switzerland: Citeseer; 2019.
- [7] Liu L, Cai G, Zhang J, Liu X, Liu K. Evaluation of engineering properties and environmental effect of recycled waste tire-sand/soil in geotechnical engineering: a compressive review. Renew Sustain Energy Rev 2020;126:109831. https://doi. org/10.1016/j.rsep.2020.109831.
- [8] Yoon S, Prezzi M, Siddiki NZ, Kim B. Construction of a test embankment using a sand-tire shred mixture as fill material. Waste Manag 2006;26(9):1033-44. https://doi.org/10.1016/j.wasman.2005.10.009.

- [9] Tsang HH. Seismic isolation by rubber-soil mixtures for developed countries. Earthq Eng Struct Dynam 2008;37(2):283–303. https://doi.org/10.1002/eqe.756.
- [10] Tsang HH, Lo SH, Xu X, Neaz Sheikh M. Seismic isolation for low-to-medium-rise buildings using granulated rubber-soil mixtures: numerical study. Earthq Eng Struct Dynam 2012;41(14):2009–24. https://doi.org/10.1002/eqe.2171.
- [11] Liu F, Ren D, Li N. Numerical simulation on the isolation effect of geocell reinforced rubber-sand mixture cushion earthquake base isolator. China Civ Eng J 2015;47:109–18.
- [12] Pitilakis K, Karapetrou S, Tsagdi K. Numerical investigation of the seismic response of RC buildings on soil replaced with rubber-sand mixtures. Soil Dynam Earthq Eng 2015;79:237–52. https://doi.org/10.1016/j.soildyn.2015.09.018.
- [13] Brunet S, de la Llera JC, Kausel E. Non-linear modeling of seismic isolation systems made of recycled tire-rubber. Soil Dynam Earthq Eng 2016;85:134–45. https://doi. org/10.1016/i.soildyn.2016.03.019.
- [14] Wu M, Liu F, Li Z, Bu G. Micromechanics of granulated rubber-soil mixtures as a cost-effective substitute for geotechnical fillings. Mech Adv Mater Struct 2023;30 (13):2701–17. https://doi.org/10.1080/15376494.2022.2062628.
- [15] Bandyopadhyay S, Sengupta A, Reddy GR. Performance of sand and shredded rubber tire mixture as a natural base isolator for earthquake protection. Earthq Eng Eng Vib 2015;14:683–93. https://doi.org/10.1007/s11803-015-0053-y.
- [16] Yin Z, Sun H, Jing L, Dong R. Geotechnical seismic isolation system based on rubber-sand mixtures for rural residence buildings: shaking table test. Materials 2022;15(21):7724. https://doi.org/10.3390/ma15217724.
- [17] Dai BB, Liu Q, Mao X, Li PY, Liang ZZ. A reinterpretation of the mechanical behavior of rubber-sand mixtures in direct shear testing. Constr Build Mater 2023; 363:129771. https://doi.org/10.1016/j.conbuildmat.2022.129771.
- [18] Liu F, Wang J, Zhou B, Wu M, He J, Bin J. Shaking table study on rubber-sand mixture cored composite block as low-cost isolation bearing for rural houses. J Build Eng 2023;76:107413. https://doi.org/10.1016/j.jobe.2023.107413.
- [19] Liu F, Zheng K, Jia B, Yang J, Wu M. Shear modulus and damping ratio of granulated rubber-sand mixtures: influence of relative particle size. Constr Build Mater 2024;427:136205. https://doi.org/10.1016/j.conbuildmat.2024.136205.
- [20] Feng ZY, Sutter KG. Dynamic properties of granulated rubber/sand mixtures. Geotech Test J 2000;23(3):338–44. https://doi.org/10.1520/gtj11055j.
- [21] Lee JS, Dodds J, Santamarina JC. Behavior of rigid-soft particle mixtures. J Mater Civ Eng 2007;19(2):179–84. https://doi.org/10.1061/(ASCE)0899-1561(2007)19: 20172.
- [22] Lee C, Truong QH, Lee W, Lee JS. Characteristics of rubber-sand particle mixtures according to size ratio. J Mater Civ Eng 2010;22(4):323–31. https://doi.org/ 10.1061/(ASCE)MT.1943-5533.0000027.
- [23] Senetakis K, Anastasiadis A, Pitilakis K. Dynamic properties of dry sand/rubber (SRM) and gravel/rubber (GRM) mixtures in a wide range of shearing strain amplitudes. Soil Dynam Earthq Eng 2012;33(1):38–53. https://doi.org/10.1016/j. soildyn.2011.10.003.
- [24] Anastasiadis A, Senetakis K, Pitilakis K. Small-strain shear modulus and damping ratio of sand-rubber and gravel-rubber mixtures. Geotech Geol Eng 2012;30: 363–82. https://doi.org/10.1007/s10706-011-9473-2.
- [25] Nakhaei A, Marandi SM, Kermani SS, Bagheripour MH. Dynamic properties of granular soils mixed with granulated rubber. Soil Dynam Earthq Eng 2012;43: 124–32. https://doi.org/10.1016/j.soildyn.2012.07.026.
- [26] Bahador H, Manafi S. Investigation on the dynamic properties of saturated sandtire chips mixture by shaking table. In: Proceedings of the 18th international conference on soil mechanics and geotechnical engineering; 2013. p. 883–6.
- [27] Ehsani M, Shariatmadari N, Mirhosseini SM. Shear modulus and damping ratio of sand-granulated rubber mixtures. J Cent S Univ 2015;22:3159–67. https://doi.org/ 10.1007/s11771-015-2853-7.
- [28] Li B, Huang M, Zeng X. Dynamic behavior and liquefaction analysis of recycled-rubber sand mixtures. J Mater Civ Eng 2016;28(11):04016122. https://doi.org/10.1061/(ASCE)MT.1943-5533.0001629.
- [29] Mashiri MS, Vinod JS, Sheikh MN. Liquefaction potential and dynamic properties of sand-tyre chip (STCh) mixtures. Geotech Test J 2016;39(1):69–79. https://doi. org/10.1520/GTJ20150031.
- [30] Madhusudhan BR, Boominathan A, Banerjee S. Static and large-strain dynamic properties of sand-rubber tire shred mixtures. J Mater Civ Eng 2017;29(10): 04017165. https://doi.org/10.1061/(ASCE)MT.1943-5533.0002016.

- [31] Okur DV, Umu SU. Dynamic properties of clean sand modified with granulated rubber. Adv Civ Eng 2018;2018(1):5209494. https://doi.org/10.1155/2018/ 5200404
- [32] Pistolas GA, Anastasiadis A, Pitilakis K. Dynamic behaviour of granular soil materials mixed with granulated rubber: effect of rubber content and granularity on the small-strain shear modulus and damping ratio. Geotech Geol Eng 2018;36: 1267–81. https://doi.org/10.1007/s10706-017-0391-9.
- [33] Sarajpoor S, Kavand A, Zogh P, Ghalandarzadeh A. Dynamic behavior of sandrubber mixtures based on hollow cylinder tests. Constr Build Mater 2020;251: 118948. https://doi.org/10.1016/j.conbuildmat.2020.118948.
- [34] Das S, Bhowmik D. Small-strain dynamic behavior of sand and sand-crumb rubber mixture for different sizes of crumb rubber particle. J Mater Civ Eng 2020;32(11): 04020334. https://doi.org/10.1061/(ASCE)MT.1943-5533.0003425.
- [35] Das S, Bhowmik D. Dynamic behaviour of sand-crumbed rubber mixture at low strain level. Geotech Geol Eng 2020;38(6):6611–22. https://doi.org/10.1007/ s10706-020-01458-4.
- [36] Li J, Cui J, Shan Y, Li Y, Ju B. Dynamic shear modulus and damping ratio of sand-rubber mixtures under large strain range. Materials 2020;13(18):4017. https://doi.org/10.3390/mai3184017.
- [37] Rios S, Kowalska M, Viana da Fonseca A. Cyclic and dynamic behavior of sand-rubber and clay-rubber mixtures. Geotech Geol Eng 2021;39(5):3449–67. https://doi.org/10.1007/s10706-021-01704-3.
- [38] Wu Q, Ma W, Liu Q, Zhao K, Chen G. Dynamic shear modulus and damping ratio of rubber-sand mixtures with a wide range of rubber content. Mater Today Commun 2021;27:102341. https://doi.org/10.1016/j.mtcomm.2021.102341.
- [39] Ghazavi M, Kavandi M. Shear modulus and damping characteristics of uniform and layered sand-rubber grain mixtures. Soil Dynam Earthq Eng 2022;162:107412. https://doi.org/10.1016/j.soildyn.2022.107412.
- [40] Banzibaganye G, Vrettos C. Resonant column tests on mixtures of different sands with coarse tyre rubber chips. Geotech Geol Eng 2022;40(12):5725–38. https://doi.org/10.1007/s10706-022-02244-0.
- [41] Wu M, Tian W, Liu F, Yang J. Dynamic behavior of geocell-reinforced rubber sand mixtures under cyclic simple shear loading. Soil Dynam Earthq Eng 2023;164: 107595. https://doi.org/10.1016/j.soildyn.2022.107595.
- [42] Kowalska M, Vrettos C. Effect of layering and pre-loading on the dynamic properties of sand-rubber specimens in resonant column tests. Acta Geotechnica 2025;20(2):607–24. https://doi.org/10.1007/s11440-024-02398-6.
- [43] GB/T 50123-2019. Standard for Soil Method. National Standard of the PRC, Beijing, CHN 2019 (in Chinese).
- [44] Wichtmann T, Triantafyllidis T. On the influence of the grain size distribution curve on P-wave velocity, constrained elastic modulus Mmax and Poisson's ratio of quartz sands. Soil Dynam Earthq Eng 2010;30(8):757–66.
- [45] Wichtmann T, Triantafyllidis T. Small-strain constrained elastic modulus of clean quartz sand with various grain size distribution. Soil Dynam Earthq Eng 2013;55: 130–9. https://doi.org/10.1016/j.soildyn.2013.08.006.
- [46] Sas W, Gabrys K. Laboratory measurement of shear stiffness in resonant column apparatus. Acta Scientiarum Polonorum. Architectura 2012;11(4).
- [47] ASTM. ASTM D4015-15 Standard test methods for modulus and damping of soils by fixed-base resonant column devices. West Conshohocken: ASTM International; 2015.
- [48] Hardin BO, Drnevich VP. Shear modulus and damping in soils: design equations and curves. J Soil Mech Found Div 1972;98(7):667–92.
- [49] Darendeli MB, Stokoe KHII. Dynamic properties of soils subjected to the 1994 northridge earthquake. Geotechnical engineering report GR97-5, civil engineering department. Austin: The University of Texas at Austin; 1997.
- [50] Wu M, Tian W, He Liu, F, Yang J J. Seismic isolation effect of rubber-sand mixture cushion under different site classes based on a simplified analysis model. Soil Dynam Earthq Eng 2023;166:107738. https://doi.org/10.1016/j. soildyn.2022.107738.
- [51] Ding Y, Zhang J, Chen X, Wang X, Jia Y. Experimental investigation on static and dynamic characteristics of granulated rubber-sand mixtures as a new railway subgrade filler. Constr Build Mater 2021;273:121955. https://doi.org/10.1016/j. conbuildmat.2020.121955.